arXiv:1510.05599v2 [cond-mat.mes-hall] 6 Jan 2016

Strong coupling regime in coherent electron transport in periodic quantum nanostructures

L. S. Petrosyan[1,2,3] and T. V. Shahbazyan[1]
[1] *Department of Physics, Jackson State University, Jackson, Mississippi 39217 USA*
[2] *Institute for Mathematics and High Technology, Russian-Armenian State University, 123 Hovsep Emin Street, Yerevan 0051, Armenia*
[3] *Department of Medical Physics, Yerevan State Medical University, 2 Koryun Street, Yerevan 0025, Armenia*

We study coherent transport in a system of a periodic linear chain of quantum dots placed between two parallel quantum wires. We show that resonant-tunneling conductance between the wires exhibits a Rabi splitting of the resonance peak as a function of Fermi energy in the wires indicating the emergence of strong coupling between the system constituents. The underlying mechanism of the strong coupling regime is conservation of the quasimomentum in a periodic system that leads to transition resonances between electron states in a quantum dot chain and quantum wires. A perpendicular magnetic field, by breaking the system's left-right symmetry, gives rise to a fine structure of the conductance lineshape.

I. INTRODUCTION

During the past decade, strong coupling effects in the optics of nanostructures have been a subject of intense interest [1]. Optical interactions between excited dye molecules or excitons in semiconductor structures and resonant optical cavity modes or surface plasmons in metal structures can lead to a mixed state with dispersion characterized by an anticrossing gap (Rabi splitting) in the resonance region. A strong coupling regime is established when the *coherent* energy exchange between two systems exceeds incoherent losses through radiative or nonradiative mechanisms, while the Rabi splitting magnitude can vary over a wide range [2–25]. For example, a relatively weak Rabi splitting in the range 100 μeV – 1 meV was reported for a semiconductor quantum dot (QD) radiatively coupled to a cavity mode [2–4], whereas a much larger splitting (above 100 meV) was observed for surface plasmons coupled to excitons in J-aggregates [5–12], individual dye molecules [13–19], or semiconductor QDs [20–22]. A weaker, although still significant, Rabi splitting ($\sim$10 meV) was reported for quantum well excitons coupled to surface-plasmon polaritons [23, 24] or to graphene plasmons [25]. Recently, strong coupling between molecular vibrational modes and cavity modes in Raman scattering experiments was reported [26–29].

On the other hand, the electron quantum transport in semiconductor nanostructures [30–32] bears deep similarities to coherent optical processes [33]. The interference of electron pathways in confined structures gives rise to, e.g., the analog of Dicke superradiance in resonant tunneling through several QDs [33, 34], Fabry-Pérot interference in electron waveguides [35], or extraordinary electron transmission through a QD lattice [36]. However, to the best of our knowledge, a physical mechanism that could give rise to a strong coupling regime in electron transport has yet to be suggested.

Here we demonstrate that a strong coupling regime can be realized in resonant tunneling through a periodic chain of QDs (QDC) [37, 38] placed between two parallel semiconductor quantum wires (QW) [39, 40] (see the inset in Fig. 1). Due to scattering by the QDC periodic potential, the energy spectrum of one-dimensional electron gas (1DEG) in QWs splits into Bloch bands that are characterized by a quasimomentum that conserves across the system. We show that even for weak tunneling between individual QDs and QWs, the momentum-selective transitions between the QDC states and Bloch states in QWs cause an anticrossing of the Bloch band dispersion and resonant energy level, leading to Rabi splitting of the conduction peak. A perpendicular magnetic field, by breaking the symmetry between the left and right QWs, leads to a fine structure of the conductance lineshape.

II. CONDUCTANCE THROUGH A PERIODIC ARRAY OF QUANTUM DOTS

We consider resonant tunneling through a QDC with lattice constant a separated from the left and right QWs by potential barriers (see Fig. 1). Within tunneling Hamiltonian formalism [33], the system Hamiltonian is

$$H=\sum_j E_0 c_j^\dagger c_j+\sum_{k\alpha}\mathcal{E}_k^\alpha c_{k\alpha}^\dagger c_{k\alpha}+\sum_{k\alpha j}\left(V_{jk}^\alpha c_j^\dagger c_{k\alpha}+\text{H.c.}\right),$$

where E_0 and $c_j^\dagger$ (c_j) are, respectively, the energy and creation (annihilation) operators for QD states, $\mathcal{E}_k^\alpha$ and $c_{k\alpha}^\dagger$ ($c_{k\alpha}$) are those for QW states with momentum k ($\alpha=L,R$ stands for the left/right QW), and V_{kj}^α is the transition matrix element between the QD and QW states. We assume no direct tunneling between QDs, and restrict ourselves to the single-electron picture of transport due to a low probability of QD double occupancy in a long chain. The zero-temperature conductance through N QDs is [33]

$$G=\frac{e^2}{\pi\hbar}\,\text{Tr}\left(\hat{\Gamma}^R\frac{1}{E_F-E_0-\hat{\Sigma}}\,\hat{\Gamma}^L\frac{1}{E_F-E_0-\hat{\Sigma}^\dagger}\right), \quad (1)$$

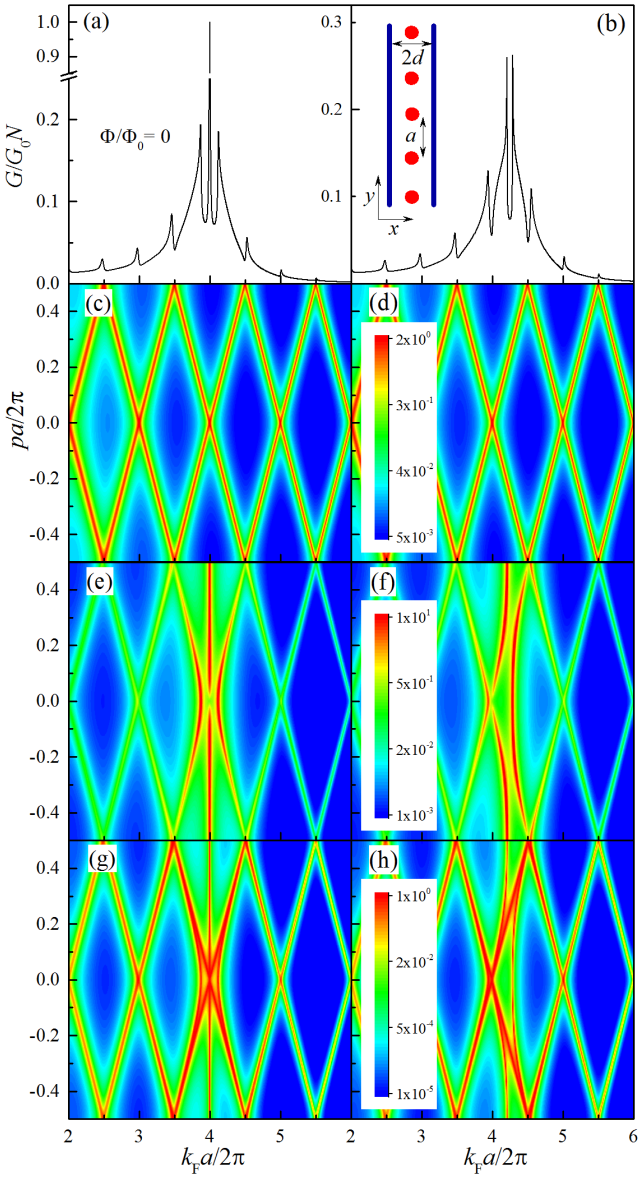

FIG. 1. Normalized per QD conductance vs. Fermi momentum k_F for resonance positions at (a) $k_F/k_a = 4.0$ and (b) $k_F/k_a = 4.25$ is shown along with the respective density plots in the (p, k_F) plane of joint tunneling rate Γ^t_p in units of Γ_a [(c) and (d)], QDC spectral function A_p in units of Γ_a^{-1} [(e) and (f)], and partial conductivity G_p [(g) and (h)]. The same color scale is used for each pair. Inset: QW/QDC/QW system schematics.

where $\Sigma_{ij} = \Sigma^L_{ij} + \Sigma^R_{ij}$ is the self-energy matrix of QDC states due to the coupling to the left and right QWs,

$$\Sigma^\alpha_{ij} = \sum_k \frac{V^\alpha_{ik} V^\alpha_{kj}}{E_F - \mathcal{E}^\alpha_k + i\gamma_\alpha} = \Delta^\alpha_{ij} - \frac{i}{2}\Gamma^\alpha_{ij}. \qquad (2)$$

Here the real and imaginary parts of Σ^α_{ij} define the energy matrix Δ^α_{ij} and the decay matrix Γ^α_{ij} and the trace is taken over N QDC sites y_j. The matrix element can be presented as $V^\alpha_{jk} = L^{-1/2} e^{iky_j} t_\alpha$, where t_α is the tunneling amplitude between QDs and QWs, and $L = Na$ is the normalization length [33, 34]. Then, the self-energy (2) takes the form $\Sigma^\alpha_{ij} = t^2_\alpha G_\alpha(y_i - y_j)$, where $G_\alpha(y_i - y_j)$ is the electron Green's function in QWs.

Due to QDC periodicity, tunneling between QDC and QWs gives rise to a quasimomentum p along the y direction that conserves across the QW/QDC/QW system [36, 41]. The 1DEG momentum space splits into Bloch bands, $k \to g_n + p$, where $g_n = k_a n$ is the nth Bloch band wave vector ($k_a = 2\pi/a$ is the reciprocal lattice vector, and n is an integer). The QDC spectrum is derived through the Fourier transform of the self-energy matrix as $\Sigma^\alpha_{ij} = N^{-1} \sum_p e^{ip(y_i - y_j)} \Sigma^\alpha_p$, where

$$\Sigma^\alpha_p = \frac{t^2_\alpha}{a} \sum_n G^\alpha_{g_n+p} = \frac{t^2_\alpha}{a} \sum_n \frac{1}{E_F - \mathcal{E}^\alpha_{g_n+p} + i\gamma_\alpha} \qquad (3)$$

is QDC self-energy in the momentum space. Here $G^\alpha_{g_n+p}$ is the QW Green's function for a band n electron with dispersion $\mathcal{E}^\alpha_{g_n+p} = \hbar^2 (g_n + p)^2 / 2m_\alpha$ and scattering rate γ_α (m_α is the electron mass). The real and imaginary parts of self-energy $\Sigma^\alpha_p = \Delta^\alpha_p - \frac{i}{2}\Gamma^\alpha_p$ determine, respectively, the QDC states' dispersion, $E_p = E_0 + \Delta^L_p + \Delta^R_p$, and decay rate, $\Gamma_p = \Gamma^L_p + \Gamma^R_p$.

A perpendicular magnetic field $\boldsymbol{B}$, included via the vector potential $\boldsymbol{A} = (0, Bx, 0)$, leads to the momentum shift $k \to k \pm (e/\hbar c) dB$ in the left and right QWs located at $x = \mp d$, respectively. In the presence of a periodic QDC potential, the Bloch bands in the left and right QWs are shifted in *opposite* directions, $k \to g^{L,R}_n(B) + p$, where

$$g^{L,R}_n(B) = k_a \left(n \pm \frac{\Phi}{2\Phi_0} \right) \qquad (4)$$

is the Bloch wave vector shifted by a magnetic flux $\Phi = 2daB$, in units of the flux quantum $\Phi_0 = hc/e$, through the elementary area enclosed by tunneling electron paths. Here, we assumed that the magnetic field does not cause any significant Zeeman splitting.

Finally, by performing the Fourier transform of Eq. (1), the conductance can be expressed in terms of the system eigenstates as $G = NG_0 k_a^{-1} \int dp\, G_p$, where

$$G_p = \Gamma^L_p S_p \Gamma^R_p S^\dagger_p = A_p \Gamma^t_p \qquad (5)$$

is the dimensionless partial conductance (transmission coefficient) of the state p, $S_p = (E_F - E_p - i\Gamma_p/2)^{-1}$ is the QDC Green's function (for brevity, $G_0 = \pi e^2/\hbar$), and p integration is taken over the Brillouin zone $(-\pi/a, \pi/a)$. To elucidate different contributions to G_p, we introduced the QDC spectral function, $A_p = -2\,\mathrm{Im}\, S_p$, and the joint tunneling rate associated with tunneling time across the system, $\Gamma^t_p = \left(1/\Gamma^L_p + 1/\Gamma^R_p\right)^{-1}$; since $\Gamma^{L,R}_p = -2\mathrm{Im}\,\Sigma^{L,R}_p$ is proportional to the left/right QW spectral function [see Eq. (3)], Γ^t_p is determined by their *overlap*.

III. NUMERICAL RESULTS AND DISCUSSION

Below we present the results of numerical calculations for a symmetric configuration, i.e., QDC at the midpoint between identical QWs ($\gamma_\alpha = \gamma$, $m_\alpha = m$, $t_\alpha = t$). The QDC period a was chosen to set $E_0 \approx 16E_a$, where $E_a = \hbar^2 k_a^2/2m$ is a geometric energy scale associated with QDC, so that the transmission resonance at $E_F = E_0$ occurs at the Fermi wave vector values $k_F \approx 4k_a$ (two values, $k_F/k_a = 4.0$ and 4.25, were used). The electron scattering rate $\gamma = \hbar v_F/l$, where v_F is the Fermi velocity and l is the scattering length, was varied in the range from $\gamma = 0.006E_0$ to $0.07E_0$ (or γ/E_a in the range $0.1 - 1.1$), yielding l/a in the range from 1 to 10; for $a \sim 100$ nm, this corresponds to a low-to-intermediate mobility in the range 10^4–10^6 cm^2/Vs. We assume that the tunneling rate between individual QDs and QWs, $\Gamma = 2mt^2/\hbar^2 k_F$ [33], is small and set $\Gamma/E_0 = 0.01$. We use the energy-independent rate $\Gamma_a = 2mt^2/\hbar^2 k_a = (k_F/k_a)\Gamma$ to describe the tunnel coupling between QDC and QWs.

In Fig. 1, we show the zero-field conductance along with density plots of Γ_p^t, A_p, and G_p in the (p, k_F) plane for a resonance position at $k_F/k_a = 4.0$ (left column) and $k_F/k_a = 4.25$ (right column). To highlight the role of Bloch bands, all curves are plotted against k_F (in units of k_a) rather than E_F. In the absence of magnetic field, the energy spectra in the left and right QWs coincide and the joint tunneling rate Γ_p^t traces Bloch bands in the (k_F, p) plane for each QW [see Figs. 1(c) or 1(d)]. The QDC spectral function A_p [Figs. 1(e) and 1(f)] peaks at resonance energy E_0 (vertical lines at $k_F/k_a = 4.0$ and 4.25, respectively) and also shows a periodic Bloch pattern due to tunnel coupling between the QDC and QW states. The striking feature is a pronounced *anticrossing* in regions of the (p, k_F) plane where, e.g., the nth Bloch band dispersion $E_F = \hbar^2(g_n + p)^2/2m$ meets the resonance at E_0. Note that for E_0 coinciding with the Bloch band center ($p = 0$), two anticrossings from the nth and $(-n)$th Bloch bands are superimposed [Fig. 1(e)], while for general E_0 anticrossings occur at two different p [Fig. 1(f)]. The partial conductance $G_p = A_p\Gamma_p^t$, shown in Figs. 1(g) and 1(h), is determined by the overlap of available states in QDC and QWs and, in fact, represents the *map of conducting states* in the (k_F, p) plane. The conductance is obtained by p integration of G_p over the Brillouin zone and shows pronounced spikes at the Brillouin zone's center ($p = 0$) and edges ($p = \pm\pi/a$) , i.e., at $k_F = \pi n/a$ [Figs. 1(a) and 1(b)]. However, the standout feature is two prominent peaks near the resonance with a peak-to-peak separation equal to the anticrossing gap in A_p.

To estimate the anticrossing gap (Rabi splitting), e.g., for $p = 0$ [Fig. 1(a)], we note that the main contribution to the electron self-energy (3) comes from two terms in the sum corresponding to $g_n = \pm nk_a$. Keeping just these terms, the resonances in A_p (for $p = 0$) are found to occur

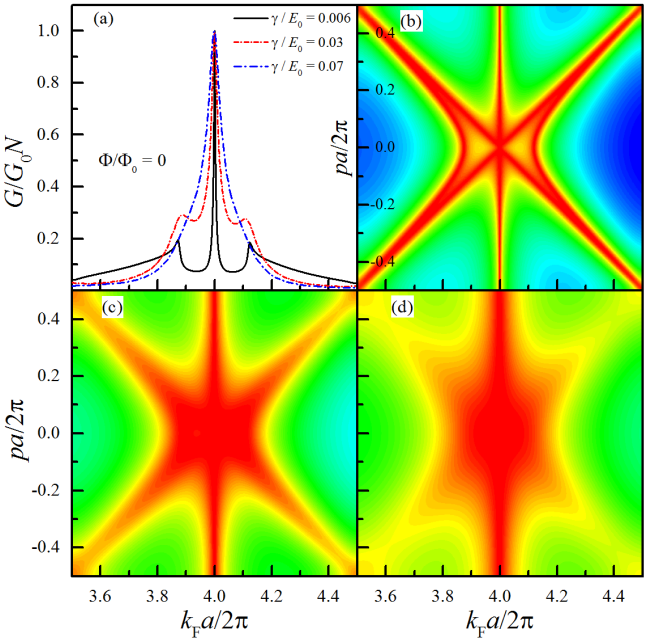

FIG. 2. (a) Normalized per QD conductance is shown with increasing γ. (b)–(d) show density plots of G_p for $\gamma/E_0 = 0.007$, 0.03, and 0.07, respectively. The same color scale for G_p as in Fig. 1 is used.

at $E_F = n^2E_a = E_0$ and $E_F = n^2E_a \pm \Delta_R$, where

$$\Delta_R = \sqrt{\frac{2}{\pi}E_a\Gamma_a - \gamma^2} \tag{6}$$

is the Rabi splitting, which indicates the onset of a strong coupling regime. Note that when plotted against k_F, the Rabi splitting is $k_F\Delta_R/2E_F$.

The emergence of a strong coupling regime in a periodic system with weak tunneling can be traced to the conservation of quasimomentum p that leads to transition resonances between the QDC and QWs at the Bloch bands' energy shell [see Eq. (3)]. Note that this momentum-selective mechanism is somewhat analogous to resonant coupling between quantum well excitons and plasmons on a metal surface [23] or in graphene [25], where in-plane momentum conservation by the Coulomb coupling leads to the anticrossing of exciton and plasmon dispersions in the momentum space. The magnitude of Rabi splitting (6) depends on the tunnel coupling Γ_a between QDC and QWs and on the electron mobility in QWs characterized by the scattering rate γ. The latter parameter determines the *effective system periodicity*, i.e., the number of QDs in the chain, $N_c = l/a$, the tunneling electron can visit before losing coherence. From Eq. (6), the onset of a strong coupling regime (i.e., $\Delta_R = 0$) can be expressed as $N_c \sim \sqrt{E_F/\Gamma_a}$, indicating that smaller tunnel coupling between QDC and QWs requires a larger electron mobility to reach the onset. In Fig. 2, we show the conductance peak evolution with

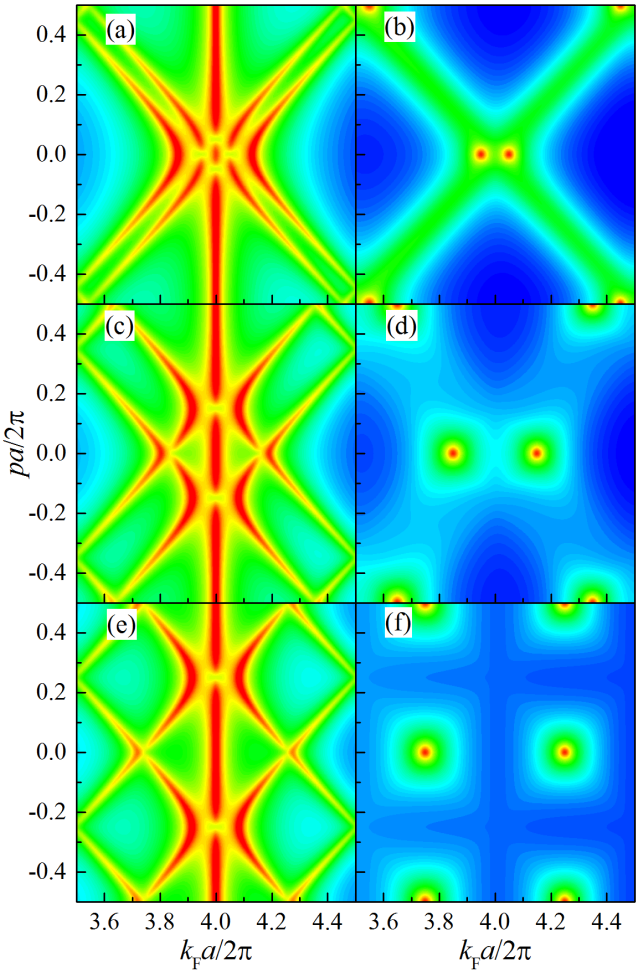

FIG. 3. Density plots of A_p (left column) and Γ_p^t (right column) are shown with increasing magnetic field for $\Phi/\Phi_0 = 0.1$ [(a) and (b)], $\Phi/\Phi_0 = 0.3$ [(c) and (d)], and $\Phi/\Phi_0 = 0.5$ [(e) and (f)]. The same color scales and units for A_p and Γ_p^t as in Fig. 1 are used.

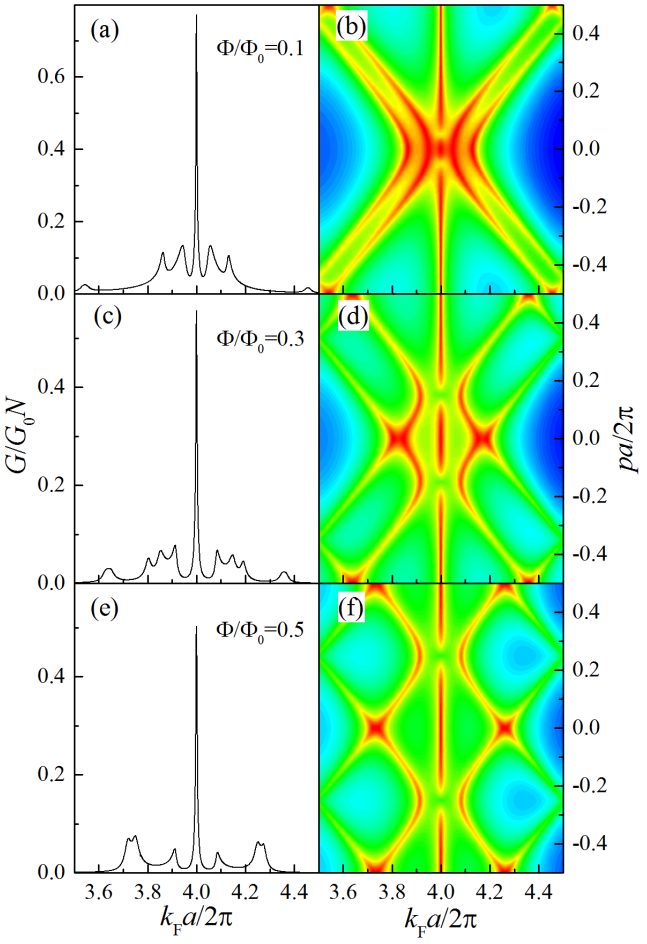

FIG. 4. Normalized per QD conductance for resonance position at $k_F/k_a = 4.0$ (left column) is shown with increasing magnetic field along with the corresponding density plot of G_p (right column). The same color scale for G_p as in Fig. 1 is used.

changing γ along with the corresponding partial conductances. With increasing γ, the anticrossing gap and hence the conductance peak Rabi splitting gradually diminish before eventually disappearing for γ exceeding the critical value.

Turning on the magnetic field shifts the left and right QW Bloch bands in the opposite directions along the p axis (see Fig. 3), leading to several anticrossings at different values of p, as shown in the A_p density plot (left column). At the same time, the overlap between the QW spectral functions, characterized by Γ_p^t, is reduced to several intersection points between the left and right QW Bloch band sets (right column). With increasing field, the anticrossings in A_p move away from each other along the p axis, following the Bloch bands' field dependence [Figs. 3(a), 3(c), and 3(e)], while the maxima of Γ_p^t move away from each other along the k_F axis [panels (b), (d), and (f)], tracking the intersection points. This results in a fine field-induced structure of the conductance lineshape, shown in Fig. 4 along with the density plot of partial conductance $G_p = A_p\Gamma_p^t$. With increasing field, the conductance develops multiple peaks as k_F changes within the Brillouin zone [Figs. 4(a), 4(c), and 4(e)] in accordance with the evolution of conducting states in the (p, k_F) plane [Figs. 4(b), 4(d), and 4(f)]. At the same time, the overall conductance magnitude is reduced due to a redistribution of the oscillator strengths between multiple peaks.

By moving the resonance position E_0 away from the Bloch band center (e.g., to $k_F/k_a = 4.25$, as shown in Fig. 5), the central conductance peak disappears (compare to Fig. 1), while the overall lineshape still exhibits multiple peaks. With increasing field, however, the resonance peak reappears [Figs. 5(c) and 5(d)] and, for $\Phi/\Phi_0 = 1/2$, it is nearly fully restored while, at the same time, the fine structure largely disappears and only a single Rabi splitting remains intact [Figs. 5(e) and 5(f)].

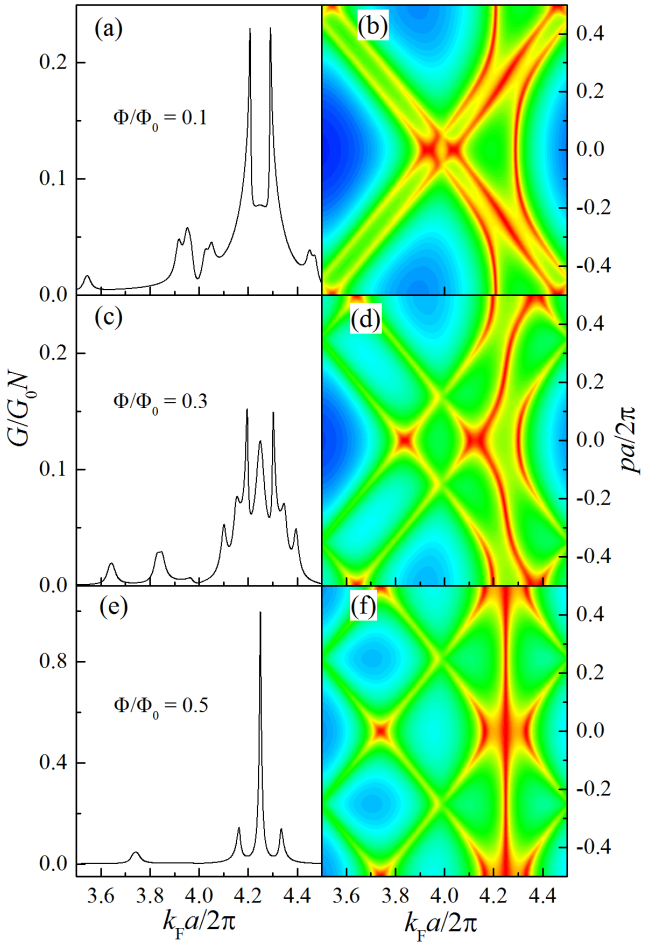

FIG. 5. Normalized conductance for resonance position at $k_F/k_a = 4.25$ (left column) is shown with increasing magnetic field along with the corresponding density plot of G_p (right column). The same color scale for G_p as in Fig. 1 is used.

This is related to the recovery of the left-right symmetry for magnetic field values satisfying $k_F = k_a|n \pm \Phi/2\Phi_0|$ [see Eq. (4)]; for such fields, both the left QW nth Bloch band and the right QW $(-n)$th Bloch band meet the resonance at the $p = 0$ point in the (p, k_F) plane [5(f)]. Note, finally, that the conductance exhibits a usual Aharonov-Bohm periodicity for integer values of Φ/Φ_0 (not shown here).

IV. CONCLUSION

In summary, we have shown that resonant tunneling conductance through a periodic chain of quantum dots placed between two parallel quantum wires can exhibit Rabi splitting of the resonance peak as a function of Fermi energy due to strong coupling between the electron states in quantum dot chain and quantum wires. The underlying mechanism of strong coupling here is the conservation of quasimomentum p that strongly enhances the transition amplitude between quantum dot chain and quantum wires when Bloch band dispersion in quantum wires approaches the quantum dot level. This novel effect in coherent transport is analogous to the Rabi splitting in optical spectra of two interacting systems caused by the anticrossing gap in the energy spectrum of mixed state. A perpendicular magnetic field breaks the symmetry between left and right quantum wires leading to a fine structure of the conductance lineshape.

ACKNOWLEDGMENTS

This work was supported by the National Science Foundation under Grant No. DMR-1206975. L.S.P. acknowledges support from the State Committee of Science, Republic of Armenia.

[1] P. Törmä and W. L. Barnes, Rep. Prog. Phys. **78**, 013901 (2015).
[2] J. P. Reithmaier, G. Sk, A. Löffler, C. Hofmann, S. Kuhn, S. Reitzenstein, L. V. Keldysh, V. D. Kulakovskii, T. L. Reinecke, and A. Forchel, Nature **432**, 197 (2004).
[3] G. Khitrova, H. M. Gibbs, M. Kira, S. W. Koch, and A. Scherer, Nature Phys. **2**, 81 (2006).
[4] K. Hennessy, A. Badolato, M. Winger, D. Gerace, M. Atatüre, S. Gulde, S. Fält, E. L. Hu, and A. Imamoglu, Nature **445**, 896 (2007).
[5] J. Bellessa, C. Bonnand, J. C. Plenet, and J. Mugnier, Phys. Rev. Lett. **93**, 036404 (2004).
[6] Y. Sugawara, T. A. Kelf, J. J. Baumberg, M. E. Abdelsalam, and P. N. Bartlett, Phys. Rev. Lett. 97, 266808 (2006).
[7] G. A. Wurtz, P. R. Evans, W. Hendren, R. Atkinson, W. Dickson, R. J. Pollard, A. V. Zayats, W. Harrison, and C. Bower, Nano Lett. **7**, 1297 (2007).
[8] N. T. Fofang, T.-H. Park, O. Neumann, N. A. Mirin, P. Nordlander, and N. J. Halas, Nano Lett. **8**, 3481 (2008).
[9] J. Bellessa, C. Symonds, K. Vynck, A. Lemaitre, A. Brioude, L. Beaur, J. C. Plenet, P. Viste, D. Felbacq, E. Cambril, and P. Valvin, Phys. Rev. B **80**, 033303 (2009).
[10] N. T. Fofang, N. K. Grady, Z. Fan, A. O. Govorov, and N. J. Halas, Nano Lett. **11**, 1556 (2011).
[11] S. Aberra Guebrou, C. Symonds, E. Homeyer, J. C. Plenet, Y. N. Gartstein, V. M. Agranovich, and J. Bellessa, Phys. Rev. Lett. 108, 066401 (2012).
[12] A. E. Schlather, N. Large, A. S. Urban, P. Nordlander, and N. J. Halas, Nano Lett. **13**, 3281 (2013).
[13] T. K. Hakala, J. J. Toppari, A. Kuzyk, M. Pettersson, H. Tikkanen, H. Kunttu, and P. Torma, Phys. Rev. Lett. **103**, 053602 (2009).
[14] A. Berrier, R. Cools, C. Arnold, P. Oermans, M. Crego-Calama, S. H. Brongersma, and J. Gomez-Rivas, ACS Nano **5**, 6226 (2011).

[15] A. Salomon, R. J. Gordon, Y. Prior, T. Seideman, and M. Sukharev, Phys. Rev. Lett. **109**, 073002 (2012).

[16] A. Gonzalez-Tudela, P. A. Huidobro, L. Martin-Moreno, C. Tejedor, and F. J. Garcia-Vidal, Phys. Rev. Lett. **110**, 126801 (2013).

[17] T. Antosiewicz, S. P. Apell, and T. Shegai, ACS Photonics, **1**, 454 (2014).

[18] A. De Luca, R. Dhama, A. R. Rashed, C. Coutant, S. Ravaine, P. Barois, M. Infusino, and G. Strangi, Appl. Phys. Lett. **104**, 103103 (2014).

[19] A Delga, J Feist, J Bravo-Abad, FJ Garcia-Vidal, Phys. Rev. Lett. **112**, 253601 (2014).

[20] D. E. Gomez, K. C. Vernon, P. Mulvaney, and T. J. Davis, Nano Lett. **10**, 274 (2010).

[21] D. E. Gomez, S. S. Lo, T. J. Davis, and G. V. Hartland, J. Phys. Chem. B **117**, 4340 (2013).

[22] A. Manjavacas, F. J. Garcia de Abajo, and P. Nordlander, Nano Lett. **11**, 2318 (2011).

[23] P. Vasa, R. Pomraenke, S. Schwieger, Y. I. Mazur, V. Kunets, P. Srinivasan, E. Johnson, J. E. Kihm, D. S. Kim, E. Runge, G. Salamo, and C. Lienau, Phys. Rev. Lett. **101**, 116801 (2008).

[24] B. J. Lawrie, K.-W. Kim, D. P. Norton, and R. F. Haglund Jr., Nano Lett. **12**, 6152 (2012).

[25] K. A. Velizhanin and T. V. Shahbazyan, Phys. Rev. B **90**, 085403 (2014).

[26] A. Shalabney, J. George, J. Hutchison, G. Pupillo, C. Genet and T. W. Ebbesen, Nature Comm. **6**, 5981 (2015).

[27] J. P. Long and B. S. Simpkins, ACS Photonics **2**, 130 (2015).

[28] A. Shalabney, J. George, H. Hiura, J. A. Hutchison, C. Genet, P. Hellwig, T. W. Ebbesen, Angew. Chem. **127**, 8082 (2015).

[29] J. del Pino, J. Feist and F. J. Garcia-Vidal, New J. Phys. **17**, 053040 (2015).

[30] A. Yacoby, M. Heiblum, D. Mahalu, and H. Shtrikman, Phys. Rev. Lett. **74**, 4047 (1995).

[31] R. Schuster, E. Buks, M. Heiblum, D. Mahalu, V. Umansky, and H. Shtrikman, Nature (London) **385**, 417 (1997).

[32] E. Buks, R. Schuster, M. Heiblum, D. Mahalu, and V. Umansky, Nature (London) **391**, 871 (1998).

[33] T. Brandes, Phys. Rep. **408**, 315 (2005).

[34] T. V. Shahbazyan and M. E. Raikh, Phys. Rev. B 49, 17123 (1994).

[35] W. Liang, M.Bockrath, D. Bozovic, J. H. Hafner, M. Tinkham, and H. Park, Nature, **411** 665 (2001).

[36] L. S. Petrosyan, A. S. Kirakosyan, and T. V. Shahbazyan, Phys. Rev. Lett. **107**, 196802 (2011).

[37] S. Bandyopadhyay, A. E. Miller, H. C. Chang, G. Banerjee, V. Yuzhakov, D.-F. Yue, R. E. Ricker, S. Jones, J. A. Eastman, E. Baugher, and M. Chandrasekhar, Nanotechnology **7** 360 (1996).

[38] J. Liang, H. Luo, R. Beresford, and J. Xu, Appl. Phys. Lett. **85**, 5974 (2004).

[39] O. M. Auslaender, A. Yacoby, R. de Picciotto, K. W. Baldwin, L. N. Pfeiffer, and K. W. West, Science **295**, 825 (2002).

[40] Y. Tserkovnyak, B. I. Halperin, O. M. Auslaender, and A. Yacoby, Phys. Rev. Lett. **89**, 136805 (2002).

[41] L. S. Petrosyan and T. V. Shahbazyan, Phys. Rev. B **91**, 045405 (2015).